

Contents lists available at ScienceDirect

Journal of Quantitative Spectroscopy & Radiative Transfer

journal homepage: www.elsevier.com/locate/jqsrt



High-temperature He- and O_2 -broadening of the R(12) line in the $1 \leftarrow 0$ band of carbon monoxide



Clayton R. Mulvihill*, Sulaiman A. Alturaifi, Eric L. Petersen

Department of Mechanical Engineering, Texas A&M University, 3123 TAMU, College Station, TX 77843, United States

ARTICLE INFO

Article history: Received 11 January 2018 Revised 14 May 2018 Accepted 18 June 2018 Available online 21 June 2018

Keywords: CO-He CO-O₂ CO fundamental band Helium broadening Oxygen broadening

ABSTRACT

Line shapes of the R(12) line in the $1\leftarrow 0$ band of CO were measured near 1 atm between 1100 and 2200 K in mixtures of helium and oxygen behind reflected shock waves. A quantum cascade laser was scanned over the R(12) line at 2190.0175 cm⁻¹ with a scan range of 0.4 cm⁻¹ and a scan rate of 2 kHz. Voigt profiles were fit to the measured line shapes. The temperature dependence of the broadening coefficient was assumed to take the form $\gamma(T) = \gamma(T_0)(T_0/T)^n$ ($T_0 = 296$ K). By extrapolating from the high-temperature data, values of 0.048 \pm 0.005 and 0.048 \pm 0.004 cm⁻¹ atm⁻¹ were obtained for $\gamma_{CO-He}(T_0)$ and $\gamma_{CO-O_2}(T_0)$, respectively, while values of 0.53 \pm 0.06 and 0.62 \pm 0.04 were obtained for n_{CO-He} and n_{CO-O_2} , respectively. For validation purposes, line shapes were also measured in argon mixtures; the resulting CO-Ar broadening parameters were in excellent agreement with recent literature values. Line shapes were also measured at room temperature in mixtures of CO/He and CO/O₂; excellent agreement was found between measured and historical values of $\gamma_{CO-He}(T_0)$ and $\gamma_{CO-O_2}(T_0)$. The general behavior of the broadening coefficient over a wide temperature range is discussed. The broadening parameters presented herein are useful for modeling CO-He and CO-O₂ broadening of the R(12), 1 \leftarrow 0 transition between 1100 and 2200 K and are the first measurements of their kind.

© 2018 Elsevier Ltd. All rights reserved.

1. Introduction

Carbon monoxide is a key intermediate species and a regulated byproduct of hydrocarbon combustion as well as a constituent of planetary atmospheres and a member of the interstellar medium [1]. Accurate, non-invasive measurements of CO concentrations via laser absorption require well-known broadening parameters for perturbing species. Molecular oxygen is a dominant perturber in Earth's atmosphere and in combustion systems, while helium is a perturber in the interstellar medium and is also frequently used as a diluent in fundamental combustion studies. CO-He broadening is of particular interest as recent shock-tube chemical kinetics studies have suggested that CO is formed in vibrational non-equilibrium during the oxidation of CH₄ [2] and CH₂O [3]. Sen et al. [2] therefore used 20% He in their mixtures to speed up vibrational relaxation of CO. However, they assumed the same high-temperature broadening coefficient for CO-He as for CO-Ar, an assumption that the present work shows to be invalid, at least for the CO transition of present interest.

Line strengths in the fundamental band of CO are ${\sim}10^2$ and ${\sim}10^4$ times greater than those in the first and second overtone

bands, respectively, making the fundamental band ideal for sensitive measurements of CO. The R(12), $1 \leftarrow 0$ line at 2190.0175 cm⁻¹ is well isolated from neighboring CO lines; has a relatively large line strength; and shows little interference from H₂O and CO₂ [4]. For these reasons, the R(12) line is useful for sensitive measurements of CO in a variety of applications.

CO–He broadening of the R(12) line has been studied by a number of workers [5–10]. Each of these studies included tests at room temperature, and thus the room-temperature broadening is well known. However, the temperature dependence has only been studied by Mantz et al. [9] and Predoi-Cross et al. [10], both of whom studied CO–He broadening at temperatures from 77–296 K. Similarly, several groups have contributed to CO–O₂ broadening of the R(12) line at room temperatures [5,11–13], leading to a consensus on the room-temperature CO–O₂ broadening coefficient. However, only Hartmann et al. [12] have provided theoretical predictions of the temperature dependence of the CO–O₂ broadening. To the best of the authors' knowledge, there are no high-temperature (> 300 K) experimental data on either CO–He or CO–O₂ broadening of the R(12) line.

Therefore, the present work reports the first measurements of high-temperature CO-He and $CO-O_2$ broadening of the R(12) line. In this paper, an overview of the relevant theory is given, followed by a description of the experimental apparatus. Sample experimen-

^{*} Corresponding author. E-mail address: cmulvihill@tamu.edu (C.R. Mulvihill).

tal results are presented, along with line strength measurements. Finally, high-temperature broadening data are presented, including a set of validation tests in a $\text{CO/H}_2/\text{Ar}$ mixture, as are room-temperature measurements. A brief discussion is given on the difference between room-temperature and high-temperature broadening parameters.

2. Theory

The spectral absorption of nearly monochromatic light by a weakly absorbing medium is described by the Beer-Lambert relation.

$$I_t/I_0 = \exp[-S\phi P_{abs}L],\tag{1}$$

which relates the transmitted (I_t) and incident (I_0) intensities to the line strength S [cm $^{-2}$ atm $^{-1}$], the line shape ϕ [cm], the partial pressure of the absorber P_{abs} [atm], and the path length L [cm]. The dependence of S on temperature T [K] is given by

$$S(T) = S(T_0) \frac{Q(T)}{Q(T_0)} \left(\frac{T_0}{T}\right) \exp\left[-\frac{hcE''}{k} \left(\frac{1}{T} - \frac{1}{T_0}\right)\right] \times \left[1 - \exp\left(-\frac{hc\nu_0}{kT}\right)\right] \left[1 - \exp\left(-\frac{hc\nu_0}{kT_0}\right)\right]^{-1}.$$
 (2)

Here, $S(T_0)$ is the line strength at reference temperature T_0 (typically 296 K), Q(T) is the partition function at T_0 , E'' is the lower-state energy [cm $^{-1}$], ν_0 is the line center [cm $^{-1}$], and h, c, and k are Planck's constant [J·s], the speed of light [cm·s $^{-1}$], and Boltzmann's constant [J·K $^{-1}$], respectively. According to the HITEMP database [14], the parameters ν_0 , $S(T_0)$, and E'' for the R(12) line have values of 2190.0175 cm $^{-1}$, 7.13 cm $^{-2}$ atm $^{-1}$, and 299.77 cm $^{-1}$, respectively.

The line shape ϕ can be modeled by a number of profiles [15]. The Voigt profile is relatively simple and well known, describing the convolution of Gaussian (Doppler broadening) and Lorentzian (collisional broadening) profiles. The shapes of the Doppler and Lorentzian profiles are determined by their collisional full width at half maximum (FWHM) values $\Delta \nu_D$ and $\Delta \nu_L$ [cm $^{-1}$], respectively, given by

$$\Delta \nu_{\rm D} = 7.162 \times 10^{-7} \nu_{\rm 0} \sqrt{T/M} \tag{3}$$

and

$$\Delta v_L = \sum_i P_i 2 \gamma_{i-i}. \tag{4}$$

Here, M is the molecular weight of the absorber [g mol⁻¹], P_j is the partial pressure of the j-th perturber [atm], and γ_{i-j} is the broadening coefficient of the i-j absorber/perturber pair [cm⁻¹atm⁻¹]. The summation extends over all j perturbers, including the absorber itself. The temperature dependence of γ_{i-j} is given by

$$\gamma_{i-j}(T) = \gamma_{i-j}(T_0) (T_0/T)^{n_{i-j}}, \tag{5}$$

where $\gamma_{i-j}(T_0)$ [cm⁻¹atm⁻¹] is the broadening coefficient at T_0 and n_{i-j} is the temperature exponent; both of these parameters are necessary to describe the broadening of spectral lines for a specific i-j pair. The line shape ϕ is normalized to have area of unity, meaning that the integrated absorbance A [cm⁻¹] can be written as

$$A = SP_{abs}L. (6)$$

The integrated absorbance is a useful parameter in that it can remove the dependence of a species or concentration measurement on the broadening parameters of the transition.

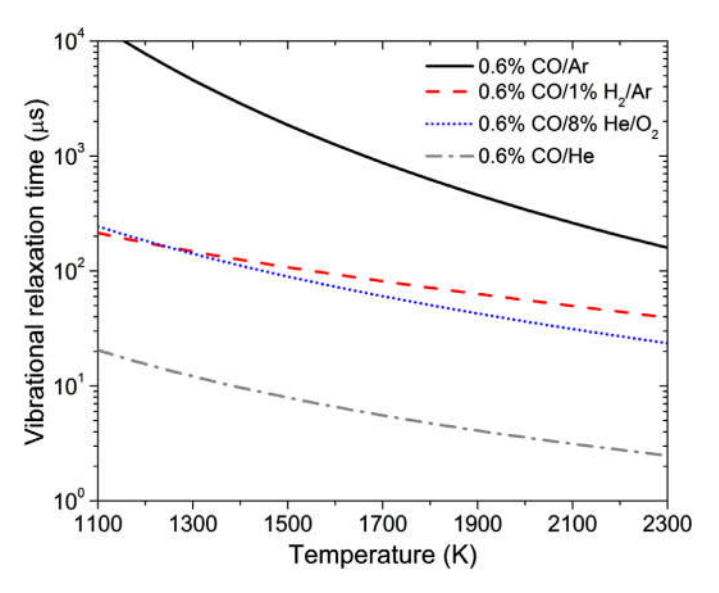


Fig. 1. Vibrational relaxation times for four mixtures at a pressure of 1.0 atm according to Millikan and White [16]. The parameter c for $CO-O_2$ relaxation, not given in [16], was assumed equal to that of $CO-H_2$ since this parameter shows "distinction between a diatomic and monatomic collision partner" [16].

3. Experiment

Experiments were performed in a high-purity, stainless steel shock tube. The driven section had a length of 4.72 m and an inner diameter of 15.24 cm, while the driver section had a length of 4.88 m and an inner diameter of 7.62 cm. Five fast-response, piezoelectric pressure transducers were used to measure the velocity of the incident shock wave over the final 180 cm of the driven section; the temperature (T_5) and pressure (P_5) behind the reflected shock wave were calculated using this measured velocity and the 1-D shock relations. The tube was pumped down to at least 1×10^{-5} Torr prior to each experiment. Mixtures were manometrically prepared in a 100-L mixing tank using a series of capacitance manometers; all mixture compositions given herein are on a by-volume basis. Gas purity levels were 99.9% for CO, 99.995% for He, and 99.999% for O2 and Ar; all gases were supplied by Praxair. Four mixtures were used to study broadening parameters: 0.6% CO/1.0% H₂/Ar, 0.6% CO/He, 0.6% CO/19.4% Ar/He, and 0.6% CO/8.0% He/O_2 .

Shock-heated CO requires a finite amount of time, τ_{vib} , to fully attain vibrational equilibrium. Estimates of τ_{vib} are shown in Fig. 1. A small amount (1%) of H₂ was added to the Ar mixture to encourage vibrational relaxation. Since H₂ would react in the presence of O₂, He was instead used in the O₂-based mixture, although a larger amount (8%) was necessary since He is a less-efficient collider than H₂. All laser scan data were acquired later than the estimated τ_{vib} , typically by at least 100 µs.

Coherent light near 2190.0 cm $^{-1}$ with a linewidth of \sim 1.5 MHz was generated by a quantum cascade laser. The laser was scanned at 2 kHz over a range of \sim 0.4 cm $^{-1}$ via injection current modulation. Two beam paths were directed onto two InSb detectors with 200 kHz bandwidths. Before terminating on the first detector, the first beam path passed through a 50.8 cm long solid germanium etalon with a free spectral range of 0.024 cm $^{-1}$. The fringes observed in this detector signal were used to determine relative changes in frequency. The second beam path, used to monitor I_0 and I_t , passed through two sapphire windows located 1.6 cm from the shock-tube endwall before terminating in the second detector. This detector was fitted with a bandpass filter (center wavelength 4562 nm, FWHM 33 nm) to reduce background emission; experi-

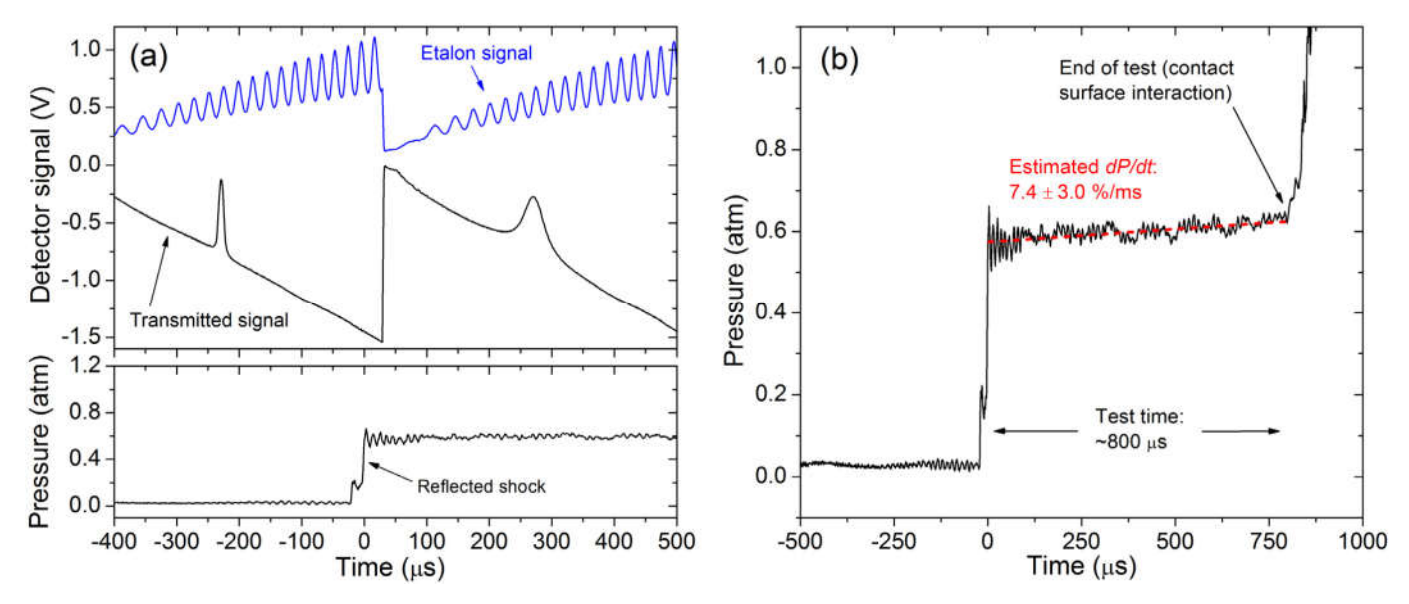


Fig. 2. (a) Sample detector (top panel) and sidewall pressure (bottom panel) traces in a mixture of 0.6% CO/He at dP/dt-corrected conditions of 1275 K, 0.593 atm. The estimated τ_{vib} is 23 μs. The etalon signal has been inverted and slightly offset for clarity. (b) Sidewall pressure trace for the same experiment, scaled to demonstrate dP/dt effects.

ments with the laser turned off confirmed that this emission was negligible (<0.1% of the absorption signal) for the conditions studied herein. Pressure measurements were recorded in the same axial plane as the sapphire windows using a high-speed pressure transducer. For more details on the laser diagnostic, see Mulvihill and Petersen [17].

Sample laser scan data are shown in Fig. 2a. As expected, the line shape at the pre-shock conditions of 296.5 K and 20.3 Torr is quite narrow. Following the passages of the incident and reflected shock waves, visible in the pressure trace, the measured line shape becomes significantly broader. Immediately before filling the shock tube with the mixture, a baseline scan was recorded; this scan was subtracted from the measured scan during data analysis to obtain the measured line shape at T_5 and P_5 . In this experiment and all others, the first available scan was taken from each experiment.

During the He-broadening experiments, non-ideal pressure rises (dP/dt) as high as 15%/ms were observed. This pressure rise (and concomitant temperature rise), while well understood in the shock-tube community, can noticeably alter post-shock conditions. To account for this, the measured pressure at the time of peak laser absorption was used in place of the nominal P_5 and the temperature calculated assuming isentropic compression of the test gas was used in place of the nominal T_5 . Isentropic compression has been shown to be a valid assumption for such calculations [18]. Fig. 2b shows a sample pressure trace at initial conditions of 1265 K, 0.581 atm. The corresponding laser scan (Fig. 2a) had peak absorption at 270 µs, leading to corrected conditions of 1275 K, 0.593 atm. All conditions reported herein for He-broadening tests are the dP/dt-corrected conditions. The Ar- and O2-broadening tests displayed much smaller values of dP/dt (typically $\leq 2\%/ms$) and thus were not dP/dt-corrected.

4. Results

4.1. Fitting of measured line shapes

For each experiment, a Voigt profile was fitted to the high-temperature scan data. Fig. 3 shows four representative line shapes, along with Voigt fits and corresponding residuals. The Voigt fits were obtained by selecting the best-fit values of S and Δv_L and also using the value of Δv_D calculated via Eq. (3). The

Ar-broadening experiments, which are included in the Supplementary Material (SM), exhibited strong signs of collisional narrowing by manner of the "gull wing" shape noted in the residuals. The O₂-broadening experiments also showed signs of collisional narrowing (e.g., Fig. 3c and d), although not to the degree noted in the Ar-broadening experiments. The He-broadening experiments performed in 0.6% CO/He showed no clear signs of collisional narrowing, even at higher temperatures (e.g., Fig. 3a and b). The He-broadening experiments in 0.6% CO/19.4% Ar/He (not shown in Fig. 3) displayed noticeable signs of collisional narrowing. These observed collisional narrowing trends accord with the idea that, in general, heavier molecules tend to promote a higher degree of collisional narrowing since a heavier mass promotes a higher number of velocity-changing collisions [19]. Included in the SM are a total of 33 measured line shapes and accompanying Voigt fits.

The best-fit values of S for the He- and O_2 -broadening experiments are compared with theoretical predictions in Fig. 4. The solid line in Fig. 4 was calculated via Eq. (2) using R(12) line parameters (v_0 , $S(T_0)$, and E'') from HITEMP [14] and values of Q(T) and $Q(T_0)$ from Laraia et al. [20], while the dashed line was calculated using line parameters from HITRAN 2016 [21] and the partition sums from Li et al. [22]. Note that the R(12) line parameters in HITEMP and HITRAN 2016 only differ in their reported values of $S(T_0)$: 2.876×10^{-19} and 2.938×10^{-19} cm⁻¹/molecule-cm⁻² for HITEMP and HITRAN 2016, respectively. Over the 1000-K range measured, the measured line strengths show good agreement with the theoretical predictions; similar agreement was observed for the Ar-broadened line strengths (not shown).

4.2. Room-temperature measurements

Direct measurements of $\gamma_{CO-He}(T_0)$ and $\gamma_{CO-O_2}(T_0)$ were also performed at room temperature. Mixtures of 0.158% CO diluted in O_2 or He were scanned at a rate of 1 kHz between 10 and 100 Torr at 299 K. Voigt fits were applied to the measured spectra; the average measured S was 7.08 cm $^{-2}$ atm $^{-1}$ (\pm 3%), which is in agreement with the HITEMP prediction of 7.12 cm $^{-2}$ atm $^{-1}$ (\pm 2-3%). Fig. 5 shows the measured values of A versus pressure for O_2 - and Hebroadening. Linear fits to the room-temperature data yield values of 0.0483 and 0.0502 cm $^{-1}$ atm $^{-1}$ for $\gamma_{CO-He}(T_0)$ and $\gamma_{CO-O_2}(T_0)$.

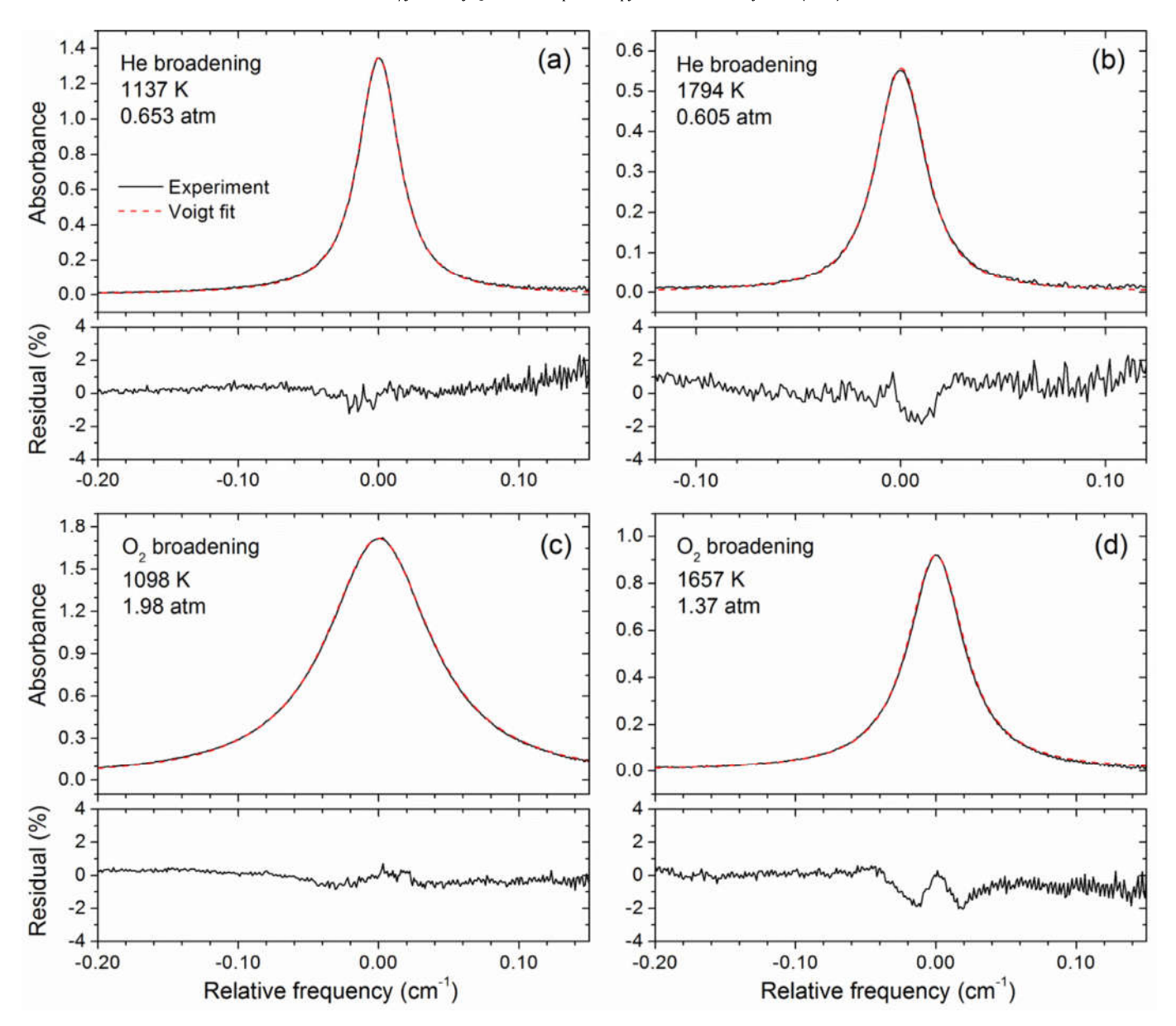


Fig. 3. Experimental line shapes, best-fit Voigt profiles, and residuals as a percent of peak absorbance in mixtures of 0.6% CO/He for (a) and (b) and 0.6% CO/8.0% He/O_2 for (c) and (d). The He broadening conditions are dP/dt-corrected.

Table 1 Historical and present values of CO–He and CO– O_2 broadening parameters.

j	$\gamma_{CO-j}(T_0)$, measured at T_0 (cm ⁻¹ atm ⁻¹)	Ref.	$\gamma_{CO-j}(T_0)$, from high-temp data (cm ⁻¹ atm ⁻¹)	Ref.	n_{CO-j}	Temp. range for n_{CO-j} (K)	Ref.
Не	$\begin{array}{c} 0.0483 \pm 0.0008 \\ 0.04712 \\ 0.04666 \pm 0.0005 \end{array}$	PW ^a [9] [7]	$0.048 \pm 0.005^{\text{b}}$	PW	0.53 ± 0.06^{b} 0.572 0.574	1100–2250 77–297 79–296	PW [9] [10]
O ₂	$\begin{array}{l} 0.0502 \pm 0.0014 \\ 0.0501 \\ 0.0502 \pm 0.0012 \end{array}$	PW [12] [13]	0.048 ± 0.004	PW	0.62 ± 0.04 0.60	1100–2250 220–3000°	PW [12]

^a PW signifies the present work.

These measured values are in close agreement with literature values, which are shown in Table 1.

Note that the room-temperature line strengths measured in the present work seem to be in better agreement with HITEMP (within 0.6%) than with HITRAN 2016 (within 2.3%). This better agreement with HITEMP was also observed by Ren et al. [4], whose value of

 $S(T_0)$ was within 0.4% of HITEMP but only within 1.8% of HITRAN 2016. Although these differences are within experimental uncertainty (2–3% in both cases), it is recommended that the HITEMP value of $S(T_0)$ be used in place of the HITRAN 2016 value for the R(12) line.

b Corresponding to "High-temp fit 2" in Fig. 6.

^c Theoretical calculations were conducted over this temperature range.

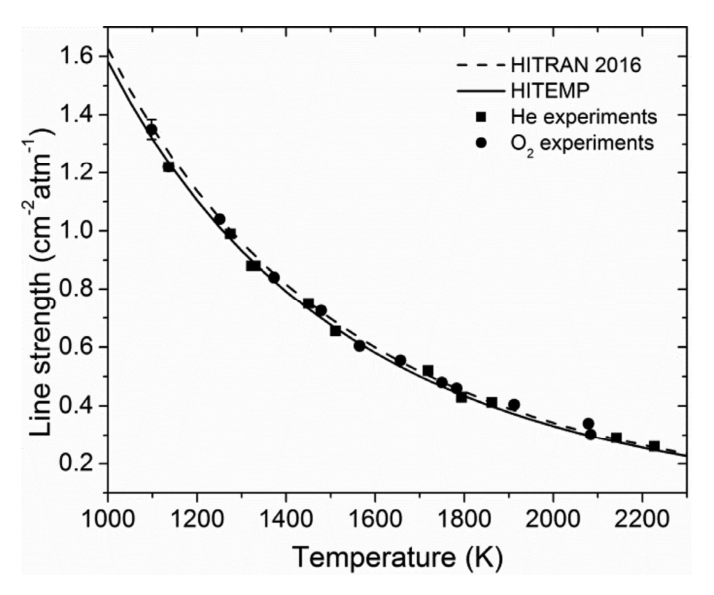


Fig. 4. Line strengths of the R(12) line as measured in He and O_2 experiments. Solid line: prediction from HITEMP [14], which uses Q(T) from Laraia et al. [20], dashed line: prediction from HITRAN 2016 [21], which uses Q(T) from Li et al. [22].

5. Discussion

5.1. High-temperature broadening coefficients

To validate the methods used herein, CO–Ar broadening measurements were performed for comparison with the recent measurements of Ren et al. [4]. A set of experiments was carried out with a mixture of 0.6% CO/1.0% H $_2$ /Ar at temperatures from 1163 to 2212 K. As in Ren et al., the broadening from CO and H $_2$ was neglected. The measured $2\gamma_{CO-Ar}$ values are shown in Fig. 6 and demonstrate excellent agreement with the Ren et al. experimental data and best fit within the estimated 3.15% uncertainty of the current measurement.

The extremely high sound speed of helium introduces several problems for shock-tube experiments. First, high sound speed causes short time intervals between the transducers used to mea-

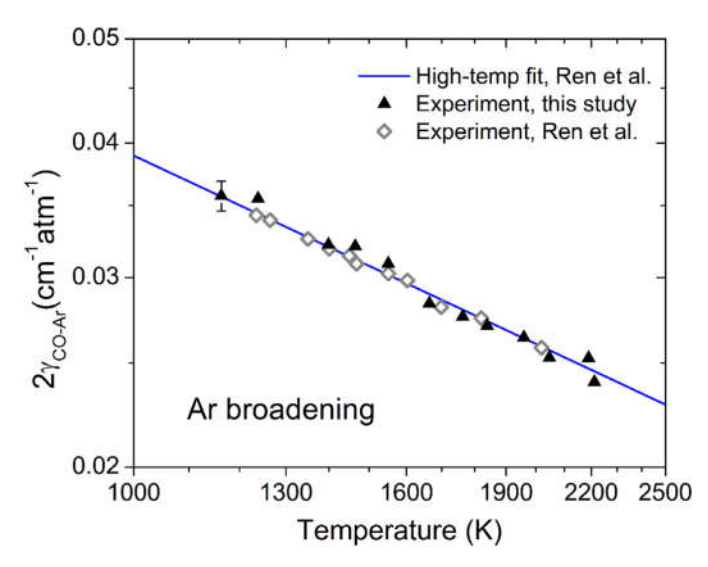


Fig. 6. Log-log plot of $2\gamma_{CO-Ar}$ values obtained in a mixture of 0.6% CO/1.0% H₂/Ar. Open diamonds: experimental data of Ren et al. [4], solid line: predictions using $\gamma_{CO-Ar}(T_0) = 0.0395 \text{ cm}^{-1} \text{atm}^{-1}$ and $n_{CO-Ar} = 0.581$, as given by Ren et al. [4].

sure shock-wave velocity, which increase uncertainty in the shock velocity and consequently in T_5 and P_5 . Second, high sound speed leads to poor shock-wave transmission, leading to lower P_5 and thus making the exact timing of the incident shock wave difficult to ascertain. Finally, high sound speed generates short test times, which make the completion of a full laser scan difficult. These problems are exacerbated at higher temperatures (i.e., at higher shock-wave velocities). To mitigate these issues, a 0.6% CO/19.4% Ar/He mixture was utilized for some experiments given that Ar has a much lower sound speed than He. This Ar-containing mixture is not shown in Fig. 1 for clarity but has a τ_{vib} that is only slightly higher (~3 µs) than the 0.6% CO/He mixture. The Ar-broadening parameters from Ren et al. [4] were used to subtract out the appropriate portion of the collisional FWHM that was due to Ar. Self-broadening by CO was neglected for all tests.

Fig. 7 shows $2\gamma_{CO-He}$ measurements for both He mixtures. Due to reasons given above, the estimated uncertainty of the

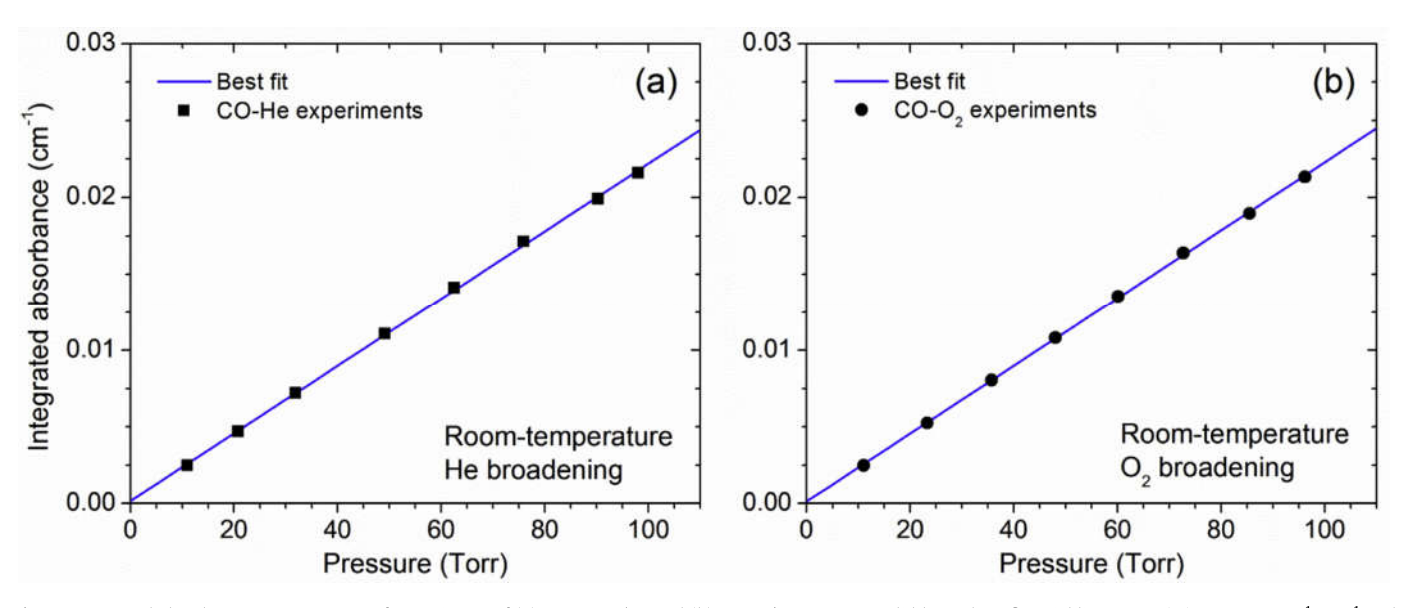


Fig. 5. Integrated absorbance versus pressure for a mixture of (a) 0.158% CO/He and (b) 0.158%/O₂ at 299 K. Solid lines: best fits, yielding $\gamma_{\text{CO}-O_2}(T_0) = 0.0502 \text{ cm}^{-1} \text{atm}^{-1}$ and $\gamma_{\text{CO}-He}(T_0) = 0.0483 \text{ cm}^{-1} \text{atm}^{-1}$.

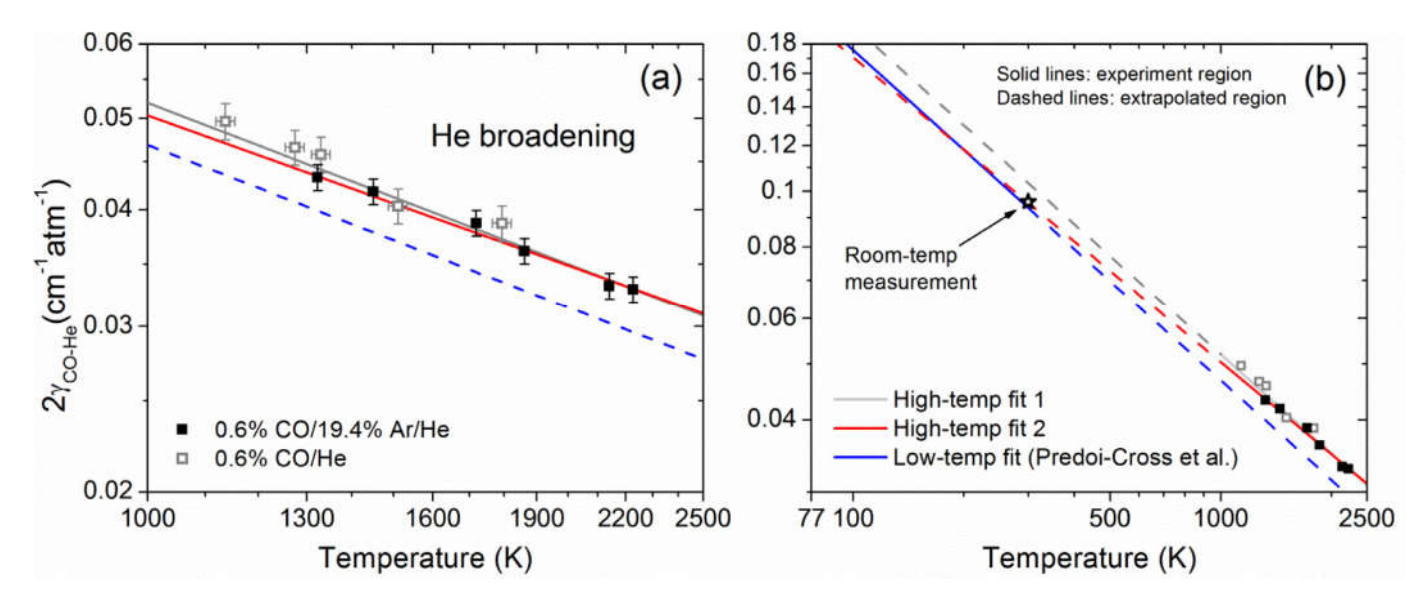


Fig. 7. Log-log plot of $2\gamma_{CO-He}$ values obtained in two different mixtures, (a) zoomed in on the high-temperature region and (b) including the low-temperature region. Red line: best fit to the 0.6% CO/19.4% Ar/He data using $\gamma_{CO-He}(T_0) = 0.048$ cm⁻¹ atm⁻¹ and $n_{CO-He} = 0.53$, gray line: alternate fit to all the data, blue line: low-temperature fit from Predoi-Cross et al. [10]. The lone star represents the room-temperature measurement from Fig. 5a. (For interpretation of the references to color in this figure legend, the reader is referred to the web version of this article.)

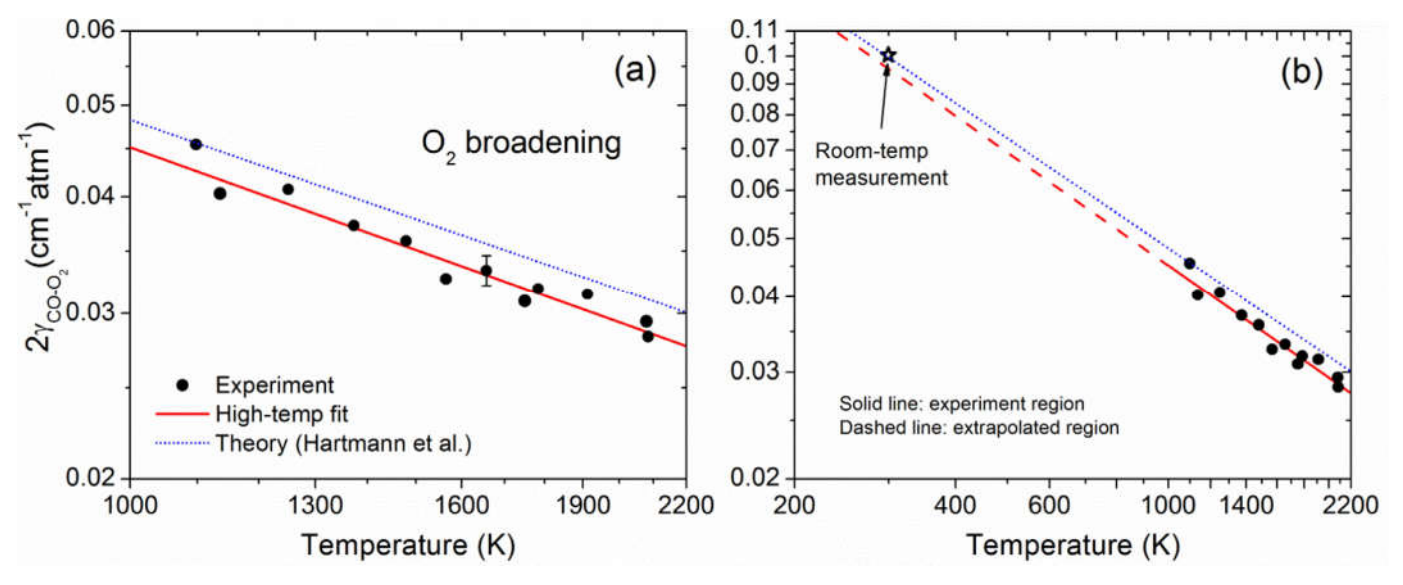


Fig. 8. Log-log plot of $2\gamma_{CO-O_2}$ values obtained in a mixture of 0.6% CO/8.0% He/O₂, (a) zoomed in on the high-temperature region and (b) including the low-temperature region. Solid line: best fit to the data using $\gamma_{CO-O_2}(T_0) = 0.048$ cm⁻¹ atm⁻¹ and $n_{CO-O_2} = 0.62$, dotted line: theory from Hartmann et al. [12]. The lone star represents the room-temperature measurement from Fig. 5b.

0.6% CO/He measurements was 4.26%, while the estimated uncertainty of the 0.6% CO/19.4% Ar/He measurements was 3.15%; see Section 5.2 for more details. The temperature uncertainty of the 0.6% CO/He data is also markedly higher than that of the 0.6% CO/19.4% Ar/He mixture. Two fits to the He data are shown in Fig. 7: a fit to both mixtures ("High-temp fit 1") and a fit to only the 0.6% CO/19.4% Ar/He data ("High-temp fit 2"). The two fits vary only slightly in the high-temperature region of Fig. 7a. However, extrapolating back to lower temperatures (Fig. 7b), one can see that "High-temp fit 1" deviates significantly from the low-temperature fit of Predoi-Cross et al. [10]. To reconcile the Predoi-Cross fit and "High-temp fit 1" would require two different power law behaviors in the intermediate temperature range (300-1000 K). However, the alternate "High-temp fit 2", obtained by setting $\gamma_{CO-He}(T_0) = 0.048 \text{ cm}^{-1} \text{atm}^{-1}$ and $n_{CO-He} = 0.53$, agrees very well with the 0.6% CO/19.4% Ar/He data and also comes into close

agreement with the Predoi-Cross fit at lower temperatures. The value of n_{CO-He} for "High-temp fit 2" is slightly lower than n_{CO-He} from Predoi-Cross, which might be in accord with the temperature exponent approaching the classical hard-sphere limit of 0.5 with increasing temperature. Note that although the 0.6% CO/He data were excluded from the "High-temp fit 2" due to their large uncertainty estimates, the given uncertainty bars can reconcile this fit with these data.

In a similar manner, measurements of $2\gamma_{\rm CO-O_2}$ were carried out in a mixture of 0.6% CO/8.0% He/O₂ and are shown in Fig. 8. As discussed earlier (Section 3), the 8% He served to hasten vibrational relaxation. The He-broadening parameters measured in the present work were used to subtract out the portion of the collisional FWHM due to He, while self-broadening of CO was neglected. The uncertainty was assumed to be 3.68%; see Section 5.2 for more information. A best fit to the $2\gamma_{\rm CO-O_2}$ data was achieved using

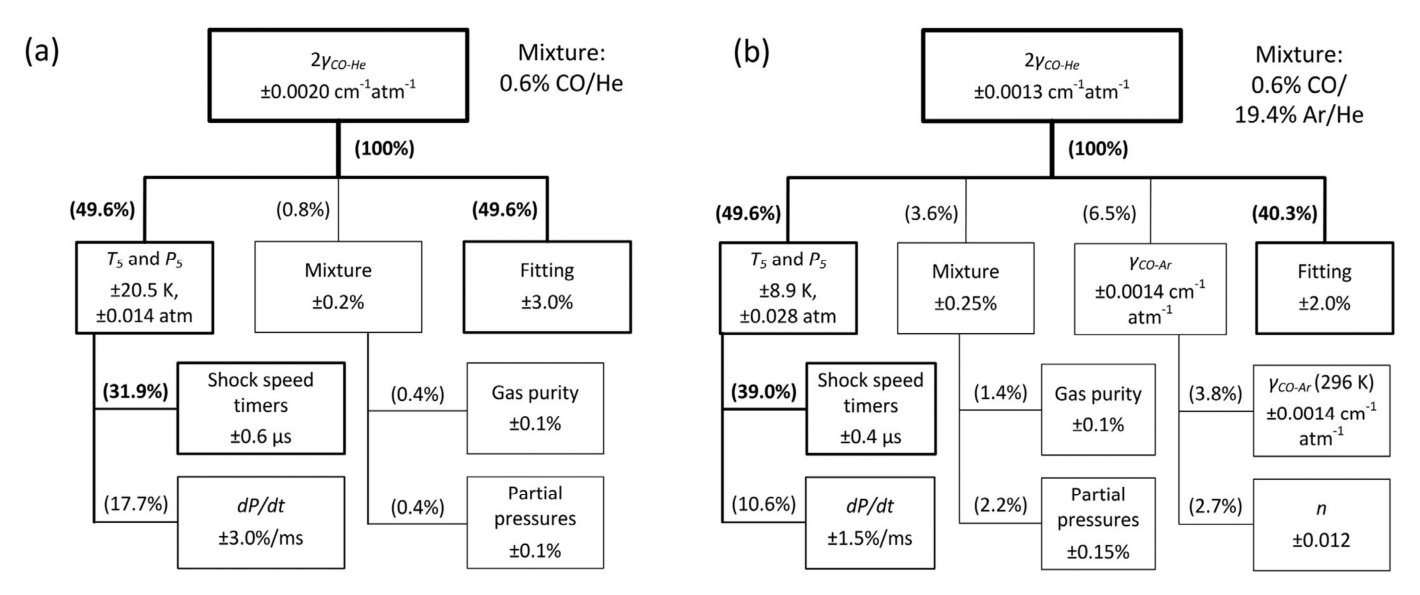


Fig. 9. Uncertainty analyses of the measured collisional widths of individual experiments in mixtures of (a) 0.6% CO/He and (b) 0.6% CO/19.4% Ar/He. Conditions are (a) 1331 K, 0.472 atm and (b) 1451 K, 2.73 atm.

 $\gamma_{CO-O_2}(T_0) = 0.048~{\rm cm^{-1}atm^{-1}}$ and $n_{CO-O_2} = 0.62$. Also shown in Fig. 8a and b is the theoretical prediction of Hartmann et al. [12], who assumed a constant value of n_{CO-O_2} over the temperature range 220–3000 K.

The various values of CO–He and CO– O_2 broadening parameters are summarized in Table 1, and two observations should be made. First, the "High-temp fit 2" proposed for the He-broadening data in Fig. 7b suggests a broadening coefficient temperature dependence that displays more than a single power law dependence over a wide temperature range. Such a possibility has been suggested previously [23], and Cybulski et al. [24] have shown analytically that broadening coefficients could certainly experience changes in slope of the kind necessitated by Fig. 7b. Second, the difference between the extrapolated and directly measured values of $\gamma_{CO-O_2}(T_0)$ is quite small. Although the differences may appear significant in Fig. 8b, these small differences fall within the uncertainty of the present work, which were obtained (for both CO–He and CO– O_2 broadening) by fitting the extreme limits of the error bars on the data.

5.2. Uncertainty analysis

To assess the sensitivity of the best-fit values of $2\gamma_{CO-j}$ to various sources of uncertainty, a detailed uncertainty analysis was performed on two experiments using the root-sum-squares method and is summarized in Fig. 9. The experiments chosen were both He-broadening experiments; one in 0.6% CO/He and one in 0.6% CO/19.4% Ar/He. In each case, the root uncertainty (at the bottom of each tree in Fig. 9) was measured, estimated, or retrieved. Then, the effect on the best-fit value of the collisional width was assessed by performing a new analysis after perturbing the uncertain variable by the specified amount.

A large source of uncertainty for both experiments is the fitting uncertainty, which is larger for the 0.6% CO/He experiment due to the lower pressure that leads to smaller linewidth and also lower absorbance. The other large source of uncertainty is the uncertainty in T_5 and P_5 , which arises primarily from uncertainty in the shock wave velocity, which is larger for the 0.6% CO/He experiment as the weak shock strength (and low P_5) makes it difficult to determine the location of the shock wave. Uncertainty in the measured value of dP/dt also contributes to uncertainty in T_5 and P_5 . Other, smaller uncertainties include mixture composi-

tion and uncertainties in the Ar-broadening coefficient. The absolute values at the top boxes of Fig. 9a and b correspond to relative uncertainties of 4.26% and 3.15%, respectively. For the Arbroadening experiments, the 3.15% uncertainty estimate obtained for the 0.6% CO/19.4% Ar/He mixture was assumed; this is likely an overestimate of the uncertainty due to the significantly slower sound speed of Ar. For the $\rm O_2$ -broadening experiments, a 1.9% uncertainty due to sensitivity of the $2\gamma_{\rm CO-O_2}$ values to uncertainty in the "High-temp fit 2" He-broadening parameters was added (via the root-sum-squares method) to the same 3.15% uncertainty estimate, yielding an estimated 3.68% uncertainty in $2\gamma_{\rm CO-O_2}$.

5.3. Implementation of broadening parameters

As previously mentioned, the R(12) line is of interest as a means to measure CO time histories in chemical kinetics experiments and has been previously utilized in such a manner on several occasions in the authors' laboratory. As the recent work of Sen et al. [2] has suggested the need to account for vibrationally unequilibrated CO, the inclusion of 20% He in chemical kinetics experiments is currently under consideration. Shown in Fig. 10 is a sample CO time history obtained during the oxidation of a fuel-lean "sour gas" (H₂S/CH₄) mixture at 99% dilution, where 20% of the mixture is He and the remaining diluent (79%) is Ar. Fig. 10 demonstrates that assuming identical broadening parameters for CO–He and CO–Ar can lead to a 7–8% error in the calculated levels of CO, demonstrating the need for accurate values of CO broadening at high temperatures for various perturbing species.

6. Conclusions

Scanned-wavelength measurements of CO–O₂ and CO–He broadening were performed at high temperatures. Voigt fits to the measured line shapes yielded collisional line widths and line shapes between temperatures of 1100 and 2200 K. The measured line strengths were found to be in excellent agreement with predictions from the HITEMP database [14]. Validation measurements of CO–Ar broadening were found to be in excellent agreement with literature measurements. The measured collisional line widths were described well by the power law $\gamma(T) = \gamma(T_0)(T_0/T)^n$. CO–O₂ and CO–He measurements were also performed at room temperature, and the measured line strengths and collisional line

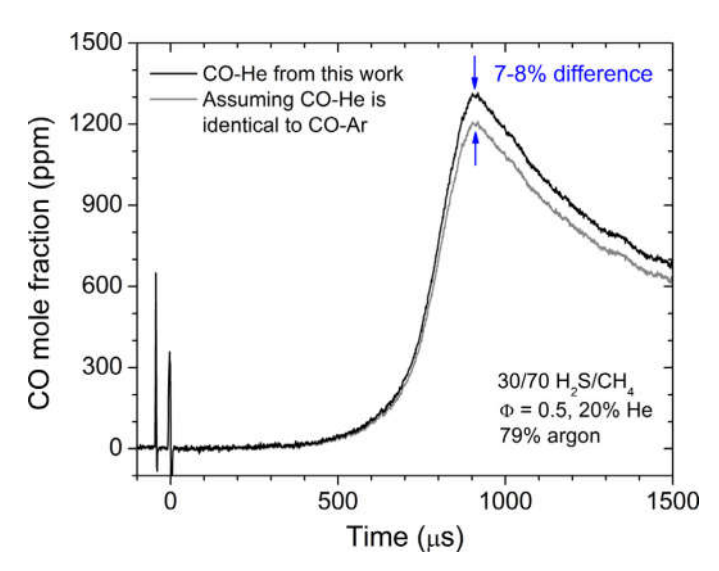


Fig. 10. Sample CO time history in a mixture of 0.0638% H₂S/0.1492% CH₄/0.787%O2/20% He/Ar. Experimental conditions are 1831 K, 1.02 atm. The gray line ignores the 20% He by assuming that the CO-He broadening is identical to the CO-Ar broadening. Data are from Mulvihill et al. [25]. (For interpretation of the references to color in this figure legend, the reader is referred to the web version of this article.)

widths were in excellent agreement with literature data. Differences between the values of $\gamma(T_0)$ when measured directly at T_0 and when extrapolated from high-temperature data were observed and discussed. The present work facilitates accurate modeling of the CO $1\leftarrow0$, R(12) line shape in the presence of O_2 and/or He in the temperature range 1100-2200 K.

Acknowledgments

This work was funded by the National Science Foundation, grant numbers DGE-1252521 and CBET-1706825, and by the Saudi Arabian Culture Mission, scholarship number 465525.

Supplementary materials

Supplementary material associated with this article can be found, in the online version, at doi:10.1016/j.jqsrt.2018.06.015.

References

[1] BelBruno JJ, Gelfand J, Rabitz H. Collision dynamical information from pressure broadening measurements: application to carbon monoxide. J Chem Phys 1983:78:6.

- [2] Sen F, Shu B, Kasper T, et al. Shock-tube and plug-flow reactor study of the oxidation of fuel-rich CH₄/O₂ mixtures enhanced with additives. Combust Flame.
- Wang S. Davidson D. Hanson K. Shock R. Tube and laser absorption study of CH2O oxidation via simultaneous measurements of OH and CO. I Phys Chem A 2017;121:45.
- [4] Ren W, Farooq A, Davidson DF, Hanson RK. CO concentration and temperature sensor for combustion gases using quantum-cascade laser absorption near 4.7 μm. App Phys B. 2012;107:2.
- Crane-Robinson C, Thompson HW. Pressure broadening studies on vibration-rotation bands, IV. Optical collision diameters for foreign-gas broadening of CO and DCI bands. Proc R Soc London Series A. 1963;272:1351.
- [6] Draegert DA, Williams D. Collisional broadening of CO absorption lines by foreign gases. J Opt Soc Am 1968;58:10.
- Sinclair PM, Duggan P, Berman R, Drummond JR, May AD. Line broadening in the fundamental band of CO in CO-He and CO-Ar mixtures. J Mol Spectr 1998:191:2.
- [8] Luo C, Wehr R, Drummond JR, et al. Shifting and broadening in the fundamental band of CO highly diluted in He and Ar: a comparison with theory. J Chem Phys 2001;115:5.
- Mantz AW, Malathy Devi V, Chris Benner D, et al. A multispectrum analysis of widths and shifts in the 2010–2260 cm⁻¹ region of ¹²C¹⁶O broadened by Helium at temperatures between 80 and 297 K. J Mol Struct 2005;742:1.
- [10] Predoi-Cross A, Esteki K, Rozario H, et al. Theoretical and revisited experimentally retrieved He-broadened line parameters of carbon monoxide in the fundamental band. J Quant Spec Rad Trans 2016;184.
- [11] Bouanich JP, Brodbeck, Mesure des C. largeurs et des deplacements des raies de la bande $0 \rightarrow 2$ de CO autoperturbe et perturbe par N_2 , O_2 , H_2 , HCl, NO et CO₂. J Quant Spec Rad Trans 1973;13:1.
- [12] Hartmann JM, Rosenmann L, Perrin MY, Taine J. Accurate calculated tabulations of CO line broadening by H₂O, N₂, O₂, and CO₂ in the 200-3000-K temperature range. App Opt 1988;27:15.
- [13] Nakazawa T, Tanaka M. Measurements of intensities and self- and foreigngas-broadened half-widths of spectral lines in the CO fundamental band. J Quant Spec Rad Trans 1982;28:5.
- [14] Rothman LS, Gordon IE, Barber RJ, et al. HITEMP, the high-temperature molecular spectroscopic database. J Quant Spec Rad Trans 2010;111:15
- Goldenstein CS, Spearrin RM, Jeffries JB, Hanson RK. Infrared laser-absorption sensing for combustion gases. Prog Energy Comb Sci 2017;60.
- [16] Millikan RC, White DR. Systematics of vibrational relaxation. J Chem Phys 1963:39:12.
- [17] Mulvihill CR, Petersen EL. High-temperature argon broadening of CO₂ near 2190 cm⁻¹ in a shock tube. App Phys B. 2017;123.
- [18] Farooq A, Jeffries JB, Hanson RK. CO₂ concentration and temperature sensor for combustion gases using diode-laser absorption near 2.7 µm. App Phys B 2008;90:3.
- [19] Pine AS. Collisional narrowing of HF fundamental band spectral lines by neon and argon. J Mol Spectr 1980;82:2.
- [20] Laraia AL, Gamache RR, Lamouroux J, Gordon IE, Rothman LS. Total internal
- partition sums to support planetary remote sensing. Icarus 2011;215:1. Gordon IE, Rothman LS, Hill C, et al. The HITRAN2016 molecular spectroscopic database. J Quant Spec Rad Trans 2017;203.
- [22] Li G, Iouli EG, Laurence SR, et al. Rovibrational line lists for nine isotopologues of the CO molecule in the $X^1\Sigma^+$ ground electronic state. The Astrophys J Suppl Ser 2015;216:1.
- [23] Pack RT. Pressure broadening of the dipole and Raman lines of CO₂ by He and Ar. Temperature dependence. J Chem Phys 1979;70.
- Cybulski H, Bielski A, Ciuryło R, Szudy J, Trawiński RS. Power-law temperature dependence of collision broadening and shift of atomic and molecular rovibronic lines. J Quant Spec Rad Trans 2013;120.
- [25] Mulvihill CR, Keesee CL, Sikes T, Teixeira RS, Mathieu O, Petersen EL. Ignition delay times, laminar flame speeds, and species time-histories in the H2S/CH4 system at atmospheric pressure. Proc Comb Inst 2018.